arXiv:astro-ph/9704152v1 15 Apr 1997

Wide ultrarelativistic plasma beam – magnetic barrier collision and astrophysical applications

V.V. Usov and M.V. Smolsky
Department of Condensed Matter Physics, Weizmann Institute, Rehovot 76100, Israel

The interaction between a wide ultrarelativistic fully-ionized plasma beam and a magnetic barrier is studied numerically. It is assumed that the plasma beam is initially homogeneous and impacts with the Lorentz factor $\Gamma_0 \gg 1$ on the barrier. The magnetic field of the barrier $\mathbf{B}_0$ is uniform and transverse to the beam velocity. When the energy densities of the beam and the magnetic field are comparable, $\alpha = 8\pi n_0 m_p c^2(\Gamma_0 - 1)/B_0^2 \sim 1$, the process of the beam – barrier interaction is strongly nonstationary, and the density of reversed protons is modulated in space by a factor of 10 or so. The modulation of reversed protons decreases with decrease of α. The beam is found to penetrate deep into the barrier provided that $\alpha > \alpha_{\rm cr}$, where $\alpha_{\rm cr}$ is about 0.4. The speed of such a penetration is subrelativistic and depends on α. Strong electric fields are generated near the front of the barrier, and electrons are accelerated in these fields up to the mean energy of protons, i.e. up to $\sim m_p c^2 \Gamma_0$. The synchrotron radiation of high-energy electrons from the front vicinity is calculated. Stationary solutions for the beam – barrier collision are considered. It is shown that such a solution may be only at $\alpha \lesssim 0.2 - 0.5$ depending on the boundary conditions for the electric field in the region of the beam – barrier interaction. Some astrophysical applications of these results are briefly discussed.

I. INTRODUCTION

There is now compelling evidence that plasma is ejected from many astronomical objects and flows away at relativistic speeds. The Lorentz factor, Γ_0, of such plasma wind is a few $\times(1-10)$ for the jets associated with active galactic nuclei [1] and $\sim 10^2 - 10^3$ or even more for the γ-ray bursters [2]. A strong magnetic field may be in the outflowing gas [3–6]. Relativistic magnetized winds can interact with an external medium (e.g., an ordinary interstellar medium). It was pointed out in Ref. [7] that such an interaction may be responsible for radiation of both X-rays and γ-rays from the γ-ray bursters. For consideration of the interaction between a relativistic magnetized wind and an external medium, it is convenient to switch to the wind frame. In this frame, the problem of the magnetized wind – external medium interaction is identical to the problem of collision between a wide relativistic beam of cold plasma and a region with a strong magnetic field which is called a magnetic barrier.

The problem of the interaction between plasma beams and magnetic barriers was attacked in many experiments and theoretical papers (see Ref. [8] and references therein). However, all known experimental studies of the beam – magnetic barrier interaction are irrelevant to our problem. This is because the plasma beams produced by the laboratory equipment are either non-relativistic or very narrow and the cross-beam sizes are much smaller than the gyroradius of the beam protons in the field of the barrier. In the theoretical studies, it is usually used the assumption of Rosenbluth [9] that the charge separation is small. However, this assumption is valid provided that the inequality $(v_0/c)^2 \ll m_e/m_p \simeq 5.4 \times 10^{-4}$ holds true, where v_0 is the beam velocity, m_e is the electron mass and m_p is the proton mass. For relativistic beams, $v_0 = c\sqrt{1-(1/\Gamma_0)^{-2}} \simeq c$, the assumption of Rosenbluth proves inadequate, and the charge separation is very important for the dynamics of particles near the barrier front [10,11]. Below, the interaction of a wide ultrarelativistic plasma beam with a magnetic barrier is considered numerically (for preliminary results and some astrophysical applications, see Ref. [11]).

II. FORMULATION OF THE PROBLEM AND BASIC EQUATIONS

The situation to be discussed is the following. At the initial moment, $t = 0$, the ultrarelativistic (Lorentz factor $\Gamma_0 \gg 1$) neutral beam of protons and electrons (number densities $n_p = n_e \equiv n_0$) runs along the x axis into the magnetic barrier which is the half-space $x > 0$ with an external magnetic field $\mathbf{B}_0 = B_0 \hat{\mathbf{e}}_z \Theta[x]$, where n_0, B_0 are constants and $\Theta[x]$ is the step function equal to unity for $x > 0$ and to zero for $x < 0$. The beam is infinite in the y – z dimensions and semi-infinite in the x dimension. Our goal is to construct a $1\frac{1}{2}$D time-dependent solution for the problem, i.e. to find induced electromagnetic fields ($\mathbf{E} = E_x \hat{\mathbf{e}}_x + E_y \hat{\mathbf{e}}_y$; $\mathbf{B} = B\hat{\mathbf{e}}_z$) and motion of the beam particles in the $x - y$ plane. The field structure and the beam particle motion are to be treated self-consistently. All the quantities are assumed to be dependent on t and x only.

As noted earlier, the strength of the magnetic fields in the astrophysical winds may be very high, especially in the winds outflowing from the γ-ray bursters [4,5]. High-energy electrons generate synchrotron radiation in these fields, and the radiation damping force which acts on the radiating electrons has to be taken into account. Since $m_p \gg m_e$, both the synchrotron radiation of protons and the radiation damping force which acts on the protons are very small (e.g., Ref. [12]) and may be neglected.

The following set of equations can be used to describe the process of the beam – barrier collision [12]:

$$\frac{\partial E_x}{\partial x} = 4\pi\rho\,, \tag{1}$$

$$\frac{\partial E_y}{\partial x} = -\frac{1}{c}\frac{\partial B}{\partial t}\,, \tag{2}$$

$$\frac{\partial B}{\partial x} = -\frac{1}{c}\frac{\partial E_y}{\partial t} - \frac{4\pi}{c}j_y\,, \tag{3}$$

$$mc\frac{du^i}{ds} = \frac{e}{c}F^{ik}u_k + \frac{2e^4}{3m^2c^5}(F_{kl}u^l)(F^{km}u_m)u^l\,, \tag{4}$$

where ρ and $\mathbf{j}$ are the densities of charges and currents respectively, e is the charge of particles, m is the mass of particles, $m = \{m_e, m_p\}$, s is the interval, $u^i = \{\Gamma, (\mathbf{v}/c)\Gamma\}$ is the four-velocity, Γ is the Lorentz factor of particles, and F^{ik} is the electromagnetic field tensor. No simplifying assumptions besides geometrical ones are exploited when rewriting Maxwell equations (1) – (3). The second term in the right-hand side of the relativistic equation of particle motion (4) is the radiation damping four-force. Following Ref. [11], only the term of the highest power in Γ is left in the damping force. This is valid for ultrarelativistic motion of particles, $\Gamma \gg 1$ (e.g., Ref. [12]).

The four-velocity u^i from Eq. (4) is related to the charge and current densities which appear in the Maxwell equations (1) – (3):

$$j^i = \{c\rho, j_x, j_y, 0\} = \sum ce\Gamma^{-1}u^i\,, \tag{5}$$

where $\sum$ means the sum over the beam particles per unitary volume.

The energy losses, I, of electrons because of their radiation in the electric and magnetic fields are computed using the following equation [12]:

$$I = \frac{2e^4}{3m_e^2c^3}\left\{\left(\mathbf{E} + \frac{1}{c}\mathbf{v}\times\mathbf{B}\right)^2 - \frac{1}{c^2}\left(\mathbf{E}\cdot\mathbf{v}\right)^2\right\}\Gamma^2\,. \tag{6}$$

To evaluate the spectrum of the radiation of electrons, we have used the following expression for the spectral intensity of synchrotron radiation [13]:

$$I_\nu = \frac{\sqrt{3}e^3B}{m_ec^2}\frac{\nu}{\nu_c}\int_{\nu/\nu_c}^{\infty}K_{5/3}(\eta)d\eta\,, \tag{7}$$

where $K_{5/3}$ is the modified Bessel functions of 5/3 order,

$$\nu_c = \frac{3eB\Gamma^2}{4\pi m_ec}\,. \tag{8}$$

In Eqs. (7) and (8), it is taken into account that in our case the velocities of particles are perpendicular to the magnetic field, $\mathbf{v} \perp \mathbf{B}$.

The initial beam number density is taken from the equation:

$$n_0m_pc^2(\Gamma_0 - 1) = \alpha\frac{B_0^2}{8\pi}\,, \tag{9}$$

where α is the dimensionless parameter. In this work we study mainly the case $\alpha \sim 1$ when the plasma flow pressure is comparable with the magnetic field pressure of the barrier. In different runs, α ranges from 0.2 to 4.

To integrate the set of equations (1) – (9), we used a macro-particle approximation in which all particles of the beam are subdivided into a large number, $\sim 10^4$, of packets. The particles within a packet are bundled together forming a large "macro-particle" which is infinitively small along the axis x and infinitively large in all directions of the y, z plane. Each packet contains either protons or electrons (for details of the numerical method, see Ref. [11]).

The examined space-time domain is the following:

$$x_{\min} < x < x_{\max} \quad \text{and} \quad 0 < t < t_{\max}\,, \tag{10}$$

where $x_{\min} = -$ a few $\times(1-10)(c/\omega_{Bp})$, $x_{\max} =$ a few $\times(1-10)(c/\omega_{Bp})$, $t_{\max} =$ a few $\times(1-10)T_p$, $T_p = 2\pi/\omega_{Bp}$ is the proton gyroperiod, and $\omega_{Bp} = eB_0/(m_pc\Gamma_0)$ and $c/\omega_{Bp} = m_pc^2\Gamma_0/(eB_0)$ are the proton gyrofrequency and gyroradius, respectively. The time step of calculations is a few $\times 10^{-6}T_p$, depending on α.

The boundary condition for E_x is $E_x\,|_{x=x_{\max}} = 0$, as $x_{\max}$ is chosen so that no beam particles penetrate deeper than $x_{\max}$ in the observed interval of time. Electromagnetic waves generated due to charge flow are allowed to escape freely from the system that is used as boundary conditions for B and E_y in Eqs. (2) and (3).

III. RESULTS OF NUMERICAL SIMULATIONS AND SCALING

The relativistic cold plasma – magnetic barrier collision is characterized by the following parameters: B_0, Γ_0 and α. The input parameters of our simulations are given in Table I. The values of B_0 and Γ_0 are chosen to be relevant to cosmological γ-ray bursters [3–5,7,11].

A. Particle dynamics and penetration of the beam particles into the barrier

The density of protons which move towards the magnetic barrier, $v_x > 0$, is almost unperturbed untill the distance to the barrier is smaller than $\sim c/\omega_{Bp}$. Reversed protons which move away from the magnetic barrier, $v_x < 0$, are bunched in the process of the beam – barrier interaction (Fig. 1). The modulation of the density of reversed protons increases with increase of α. Namely, the ratio of the maximum to minimum densities of reversed protons is ~ 2 at $\alpha \simeq 0.2$ and ~ 10 at $\alpha \simeq 1$. A typical length of such a modulation is roughly the proton gyroradius c/ω_{Bp}. Similar phenomena was observed also in numerical simulations of collisionless shock waves near the shock front (e.g., Ref. [14]).

At $\alpha \sim 1$, the mean Lorentz factor of reversed protons that far enough from the barrier, $x < -(c/\omega_{Bp})$, where the process of strong interaction between particles and fields is more or less over, is $\langle \Gamma_p^{\rm out} \rangle \simeq (0.5 \pm 0.1)\Gamma_0$, i.e. about half of the initial kinetic energy of protons is lost in the process of their collision with the barrier (see Table II). Figure 2 shows the energy distribution for reversed protons.

The density of electrons which move away from the barrier is well correlated with the density of reversed protons; the correlation coefficient is $r \simeq 0.8$, where $r = \sigma_{pe}/\sqrt{\sigma_{pp}\sigma_{ee}}$, and

$$\sigma_{ij} = \int_{x_{\rm min}}^{x_{\rm max}} (n_i - \overline{n_i})(n_j - \overline{n_j}) dx\,, \quad \{i, j\} = \{e, p\}\,. \quad (11)$$

These electrons screen the electrostatic field, E_x, of proton bunches mostly, but not completely.

At $\alpha > \alpha_{\rm cr}$, $\alpha_{\rm cr} \simeq 0.4$, it is observed that the length of the beam particle penetration into the barrier increases in time. Figure 3 shows the x coordinate, $x_{\rm pen}$, of the most deeply penetrated proton as a function of time t. The speed of such a proton along the x axis varies strongly one from another. However, the mean velocity, $v_{\rm pen} = \langle v_x \rangle$, of the penetrated protons remains more or less constant within the studied time intervals, where $\langle v_x \rangle$ is the proton velocity which is averaged over proton gyroperiod. The value of $v_{\rm pen}$ depends on α and is equal to zero (no penetration) at $\alpha < \alpha_{\rm cr} \simeq 0.4$ (see Fig. 3 and Table III).

In the region $x < x_{\rm pen}$, strong longitudinal (E_x) and transverse (E_y, B_z) electromagnetic waves propagate while almost no remnants of the external magnetic field $B_0\Theta[x]$ are found (Fig. 4). Roughly, it could be stated that at $\alpha > \alpha_{\rm cr}$ the magnetic barrier is pushed according to the law $B(t) = B_0\Theta[x - x_{\rm pen}(t)]$ and $x_{\rm pen}$ appears to be a location of the barrier front at the moment t as well as the particle penetration depth. At $x > x_{\rm pen}$, the magnetic field remains unchanged except for its time-space variations due to low-frequency electromagnetic waves which are generated by the time-variable currents $\mathbf{j}$ in the front vicinity. At $\alpha \sim 1$, the typical amplitude of these waves is $\tilde{B}_0 \simeq (0.2 - 0.3)B_0$.

In the case $\alpha < \alpha_{\rm cr}$, when the ion penetration length does not increase with time, all protons move along the same track with small deviations from it. In this case, the velocity of all reversed protons is perpendicular to the barrier front. However, at $\alpha > \alpha_{\rm cr}$ the trajectories of protons differ qualitatively one from another (for the angular distribution of reversed protons in this case, see Fig. 5). Therefore, the dimensionless density α may be called a "stochastization parameter" of the beam protons. In all runs, the trajectories of electrons are very chaotic and differ one from another qualitatively.

B. Acceleration of electrons and high-frequency radiation

The most important feature of the dynamics of electrons is that they are accelerated in the barrier front vicinity by induced electric fields and, thus, accumulate substantial portion of the kinetic energy of protons (see Fig. 6 and Table II). Figure 7 shows the energy spectrum of outflowing electrons, $v_x < 0$, in run N. At $\alpha \sim 1$, the mean Lorentz factor of outflowing electrons and their maximum Lorentz factor far enough from the barrier, $x < -(c/\omega_{Bp})$, are

$$\langle \Gamma_e^{\rm out} \rangle \simeq 0.05 \left(\frac{m_p}{m_e}\right) \Gamma_0, \quad \Gamma_{e,{\rm max}}^{\rm out} \simeq \frac{1}{2} \left(\frac{m_p}{m_e}\right) \Gamma_0 \quad (12)$$

within a factor of 2. The fraction of the kinetic energy of relativistic protons which is transformed into the energy of outflowing electrons is up to $\sim 10\%$. The rest of the energy that is lost by protons is transformed into both low-frequency electromagnetic waves and synchrotron high-frequency radiation.

The synchrotron high-frequency radiation is generated by single electrons in the process of their ultrarelativistic motion in the electromagnetic fields. The mean energy of so-called radiating electrons near by the barrier front, $x > -(c/\omega_{Bp})$, is several times higher than the mean energy of outflowing electrons far from the barrier, $x < -(c/\omega_{Bp})$, i.e. $\langle \Gamma_e^{\rm rad} \rangle \simeq (3 - 5)\langle \Gamma_e^{\rm out} \rangle$ (see Table II). The radiating electrons are responsible for generation of the main part of the synchrotron high-frequency emission.

If the average fraction, ξ_γ, of the kinetic energy of the plasma beam that is radiated in the vicinity of the magnetic barrier is small, $\xi_\gamma < 0.01$ or $\Gamma_0^2 B_0 < 3 \times 10^8$ G, the results of our simulations for $\alpha \sim 1$ may be fitted by the following analytic expression:

$$\xi_\gamma \simeq 3 \times 10^{-4} (\Gamma_0/10^2)^2 (B_0/10^3\,{\rm G})\,. \quad (13)$$

At $\Gamma_0^2 B_0 \gg 10^8$ G, the value of ξ_γ tends asymptotically to ~ 0.15 as $\Gamma_0^2 B_0$ increases. The characteristic energy of synchrotron photons is

$$\langle \varepsilon_\gamma \rangle \simeq 3(\xi_\gamma/10^{-2}) \text{ MeV} \tag{14}$$

within a factor of 2 or so. Except for numerical factors, Eqs. (13) and (14) can be derived analytically from Eqs. (1) – (9).

At $\alpha \ll 1$, electromagnetic fields which are induced in the process of the beam – barrier collision are much smaller than B_0, and the beam particles may be treated as test particles in the field of the barrier. In this case, there is almost no energy transfer from protons to electrons. Therefore, it is natural that both acceleration of electrons and their high-frequency radiation are strongly suppressed at $\alpha \ll 1$ as was observed in our simulations (see Table II). Preliminary, we have the following scaling laws: $\langle \Gamma_e^{\rm out} \rangle \propto \alpha$, $\Gamma_{\rm e,max}^{\rm out} \propto \alpha$, $\langle \Gamma_e^{\rm rad} \rangle \propto \alpha$, $\xi_\gamma \propto \alpha^2$ and $\langle \varepsilon_\gamma \rangle \propto \alpha^2$.

We did not observe any decrease in both nonstationarity of the process of the beam – barrier interaction and in acceleration of electrons, even in simulations extended up to $t_{\rm max} \simeq 16T_p$ (see Figs. 1 and 6).

IV. STATIONARY COLLISION

The problem of the beam – barrier collision is simplified significantly if it is treated as a stationary one. This is because in a stationary consideration a time-dependence of all values is disregarded, and the beam particles of any kind (protons or electrons) move along exactly the same track. In this Section we consider the beam – barrier interaction in a stationary manner.

A fully relativistic self-consistent model of stationary interaction between a wide plasma beam and a magnetic barrier was developed by Peter, Ron and Rostocker in their pioneering paper [10]. The set of equations which describes such an interaction is [10]

$$\frac{dB_z}{dx} = A_y \left(\frac{m_e/m_p}{\sqrt{z_p}} + \frac{1}{\sqrt{z_e}} \right), \tag{15}$$

$$\frac{dE_x}{dx} = \frac{\Gamma_p}{\sqrt{z_p}} - \frac{\Gamma_e}{\sqrt{z_e}}, \tag{16}$$

$$\frac{d\phi}{dx} = -E_x, \qquad \frac{dA_y}{dx} = B_z, \tag{17}$$

where $\Gamma_j \equiv \Gamma_0 - \mu_j \phi$, $z_j \equiv \Gamma_j^2 - \mu_j^2 A_y^2 - 1$,

$$\mu_j \equiv \begin{cases} -1 & \text{for electrons } (j = e), \\ m_e/m_p & \text{for protons } (j = p), \end{cases} \tag{18}$$

ϕ and A_y are the electrostatic and magnetic potentials in units of e/mc^2. In these equations we have measured the distance x in terms of $\sqrt{2}(\omega_{pe}\beta_0/c)$, where $\omega_{pe} = (4\pi n_0 e^2/m_e)^{1/2}$ is the electron plasma frequency and $\beta_0 = v_0/c$.

Eqs. (15) and (16) for the magnetic and electric fields are first order ordinary differential equations. Strictly speaking, such an equation allows only one boundary condition. For the magnetic field B_z, the boundary condition is $B_z = B_0$ at the proton turning point x_p (see Fig. 8), where B_0 is the field of the barrier. The strength of the magnetic field B_f at the front of the barrier, $x = 0$, has to be found from integration of Eq. (15). An important issue is *where* the electric field E_x should vanish: at the right or left boundary of the collision regin $0 \le x \le x_p$. In the paper [10], the electric field vanishes at $x = x_p$, $E_x|_{x=x_p} = 0$. This seems quite natural and corresponds to our nonstationary solution. However, in Ref. [10] it is wrongly suggested that if the beam density is high enough the electric field E_x is zero at the left boundary as well, $E_x|_{x=0} = 0$. Below, stationary solutions for the beam – barrier collision are considered in detail, and, in particular, it is shown that there is a net charge in the region $0 \le x \le x_p$ irrespective of the beam density untill the beam – barrier collision is stationary, i.e. the transverse electric field E_x cannot be zero at the both boundaries at once.

The right-hand side of Eqs. (15) and (16) for the derivatives of the electric an magnetic fields contains terms which tend to infinity at the electron and proton turning points, i.e. at both $x = x_e$ and $x = x_p$. This is the main difficulty which does not permit to apply a standard numerical technique to integration of Eqs. (15) and (16) directly. Since the electric and magnetic fields should remain finite everywhere, the mentioned singularities are integrable. To integrate a set of equations with such a weak, integrable singularity, one should switch to another independent variable so that all derivatives with respect to this new variable are finite. The interval of the beam particles may be used as such a new independent variable instead of x. In this case, the right-hand sides of Eqs. (15) and (16) are finite everywhere. This is because the particle density per unitary interval is constant (e.g., Ref. [10]), rather than infinite at the turning points if measured per unitary x. We integrated Eqs. (15) – (17) from $x = 0$ to $x = x_e$ using the *electron* interval s_e as an independent variable. Then, we switched to another independent variable, s_p, which is the *proton* interval measured from the *electron* turning point with the initial condition $s_p|_{x=x_e} = s_e|_{x=x_e}$. We thus broke the region of integration into two parts and used a different independent variable for each sub-interval to integrate Eqs. (15) – (17). Then, we switched back to x as an independent variable to present results of this integration.

Following Ref. [10], we have used the dimensionless parameter $\alpha_f = 8\pi n_0 m_p c^2 \sqrt{\Gamma_0^2 - 1}/B_f^2$ as a measure of the beam density instead of α. The parameter α_f is more convenient than α for integration of Eqs. (15) – (17) because such integration is performed from $x = 0$ to $x = x_p$. In our calculations the value of α_f varies in a wide range from 10^{-2} to 10^3.

To integrate Eq. (16), the following two kinds of a boundary condition for E_x were specified: $E_x|_{x=0} = 0$ or $E_x|_{x=x_p} = 0$. Integration of Eq. (16) for the boundary condition $E_x|_{x=x_p} = 0$ was carried out with a "shooting method" technique. The electric field was guessed at the left boundary, $x = 0$, and Eq. (16) was integrated with all the quantities specified on that boundary. Then, the electric field on the left boundary was adjusted to give a closer agreement with the boundary condition $E_x|_{x=x_p} = 0$. Such shots were repeated untill the boundary condition for the electric field was satisfied with a desirable accuracy. As a rule, only a few shots were required to reach the accuracy of $\sim 1\%$.

The computational engine we used to solve the regularized set of equations was "LSODE" package [15] together with the "OCTAVE" interpreter [16]. The developed octave script is mostly compatible with the popular MatLab [17] language.

Figure 9 shows typical numerical solutions for the longitudinal electric field E_x, the magnetic field B_z and the x component of the four-velocity of electrons $u_{e,x}$ in run SR10. In this run, the boundary condition for E_x is $E_x|_{x=x_p} = 0$. The energies of both electrons and protons inside of the barrier are shown in Fig. 10. The results of our calculations are summarized in Tables IV and V. From these Tables and Fig. 9 we can see that the electric field E_x is not equal to zero at $x = 0$ and $x = x_p$ at once, as mentioned above. A common feature of all stationary solutions is that the electric and magnetic fields sharply increase near the electron turning point x_e as it was pointed out in Ref. [10]. There is the following tendency: the greater the value of α_f is, the sharper the rise of the fields is. Due to the change of independent variables discussed above, the sharp rise of the fields at the electron turning point is well-resolved: it covers a large number of integration points and derivatives of the fields with respect to the new independent variable remain finite (see Fig. 11). The later facts allow us to claim a high accuracy of our calculations.

In the paper of Peter et al. [10], Eqs. (15) – (17) were integrated directly using x as an independent variable, and, therefore, they ran into serious difficulties on their way [18] which led to certain mistakes. For example, they were not able to calculate the value $E_x(x)$ at $x = x_e$ directly, and the integration of Eq. (16) was treated as a two-point boundary value problem, adjusting $E_x(x_e)$ to be equal to zero at the both boundaries, $E_x(0) = E_x(x_p) = 0$. Our calculations show that such an adjustment is impossible (see Tables IV and V). The authors of Ref. [10] believed that at $\alpha_f \gg 1$ the orbit of electrons is strongly elongated in the y direction in a narrow vicinity of the electron turning point, and the beam electrons move more or less along the barrier front with $x \simeq x_e$ for a long time. As a result, a net charge in the collision region might be zero. We did not observe such a strong elongation of the electron orbit. Moreover, for the boundary condition $E_x|_{x=0} = 0$ we have $\alpha_f \lesssim 1$, i.e. for this boundary condition α_f cannot be much more than unit.

We have confirmed the suggestion of Ref. [10] that electrons of the beam may be strongly accelerated inside the barrier. However, such an acceleration was observed only in runs with the boundary condition for E_x in the form $E_x|_{x=x_p} = 0$. For the boundary condition $E_x|_{x=0} = 0$, the beam electrons do not penetrate substantially deeper into the barrier than their gyroradius in the field B_f, and their acceleration is very small.

For the boundary condition $E_x|_{x=x_p} = 0$, a stationary solution of Eqs. (15) – (17) can exist for any nonzero value of α_f. For all these solutions, we have $\alpha \lesssim 0.5$ (see Fig. 12). This upper limit on α is more or less evident since in a stationary case the ram pressure of the beam cannot be more than the magnetic field pressure of the barrier. As to the case of the boundary condition $E_x|_{x=0} = 0$, a stationary solution can exist only if $\alpha_f \lesssim 1$ and $\alpha \lesssim 0.2$. This reduction of the upper limit on α occurs because in such a solution the electric field E_x far enough from the barrier front is directed inside the barrier, $E_x > 0$ at $x \gtrsim$ a few $\times x_e$. This field causes protons to penetrate even deeper into the barrier and to generate even stronger electric field. At $\alpha_f > 1$, at some distance from the barrier front the electric field inside the collision region is stronger than the magnetic field, and the barrier cannot suppress penetration of protons inside itself.

V. DISCUSSION

One of the main results of our time-dependent simulations which are presented in Sec. III is that the outflowing electrons are strongly accelerated near the barrier front and accumulate substantial portion of the kinetic energy of protons. At $\alpha \sim 1$, when the ram pressure of the beam is equal about the magnetic field pressure of the barrier, the fraction of the kinetic energy of protons that is transferred to outgoing electrons is up to $\sim 10\%$. The acceleration of outflowing electrons is completely due to nonstationarity of electromagnetic fields which are induced inside and near the barrier during the beam – barrier interaction. Indeed, in a stationary case the electric field is constant in time and depends on the x coordinate only, $\mathbf{E} = \{E_x(x), 0, 0\}$. If, as in both Ref. [10] and Sec. IV, the energy losses of electrons due to their radiation inside the barrier are ignored, the electron energy is a function of x only, and the energy of reversed electrons outside the barrier coincides with their initial energy before the beam – barrier collision.

The bunching of reversed protons is a key element of nonstationarity of the beam – barrier collision. Roughly, the process of bunch formation may be illustrated in the following way. The first protons, which are entered into the barrier from $t = 0$ to $t \ll T_p$, run along almost semicircle trajectory in almost unperturbed field of the magnetic barrier. For the same Lorentz-factor, the gyroradius of electrons is much smaller than the gyroradius of protons. Therefore, electrons can not penetrate as deep as protons into the barrier. The separation of electric charges induce a strong electric field E_x in the x direction according to Eq. (1). The following protons feel this electric field. The field E_x decelerates protons and accelerates electrons. Protons that are injected into the barrier later run along "shorter" trajectories and spend less time inside the barrier. As a result, in about half of a proton gyroperiod, $t \sim \frac{1}{2}T_p$, most of the protons quit the barrier almost simultaneously, and formation of the second bunch begins, and so on.

In case of large α, the velocities, v_x, of reversed protons in the x direction are quite different (see Fig. 5) so that the bunches will decay at some distance from the barrier. Once there is no bunching at all in low α case, no bunches can be observed far from the barrier no matter what α is considered.

The propagation of plasma beams across a magnetic field is one of the oldest problems in plasma physics. In spite of the long history of investigation (e.g., Ref. [8]), a clear model of this phenomenon has yet to emerge. However, some general conclusions about the beam – magnetic field interaction were done many years ago. For example, if the plasma flow pressure is more than the magnetic field pressure, it is possible for the plasma to cross the field by purely magnetohydrodynamic principles. This propagation mode is equivalent to the motion of a solid conductor across the field. During propagation, the plasma beam picks up and carries along the ambient plasma and magnetic field. Such models of the beam propagation into the magnetic field are based on the diamagnetic properties of the plasma. Most probably, in our time-dependent simulations we observed such a propagation mode. Physically, the pushing of the magnetic field is provided by strong transverse electric currents (j_y) in the domain $x_{\rm pen}(t) - (c/\omega_{Bp}) < x < x_{\rm pen}(t)$, where $x_{\rm pen}(t)$ is the x coordinate of the most deeply penetrated particle. If α is large enough, $\alpha > \alpha_{\rm cr}$, this current layer screens strongly the external magnetic field of the barrier at $x < x_{\rm pen}(t) - (c/\omega_{Bp})$, and moves deeper and deeper into the barrier. From our time-dependent simulations, we have $\alpha_{\rm cr} \simeq 0.4$. This is more or less consistent with the conclusion that there are no stationary solutions for the beam – barrier collision if α is more than $\sim (0.2-0.5)$ depending on the boundary condition on the field E_x.

Many important features of our nonstationary solutions are absent in a stationary one. They are energy transfer from incoming protons to outgoing electrons, bunching of outgoing protons, excitation of low-frequency electromagnetic waves, etc.

The main question which remains open untill now is what the final state of the beam – barrier system in a very long-time run, $t \gg T_p$, is. As noted, we did not observe any decay of non-stationarity of the beam – barrier interaction, even in simulations extended up to $t_{\rm max} \simeq 16T_p$. However, it is possible that at $t \gg 10T_p$ our nonstationary solution tends to a stationary one. It is worth noting that a stationary solution of the beam – barrier collision might be unstable if α is high enough. Indeed, the energy of electrons inside the barrier may be a few hundred times higher than their initial energy. In this case, small ($\sim 10^{-2}$) perturbations might result in that some part of reversed, $v_x < 0$, electrons is stopped and captured inside the barrier before reaching the barrier front. Besides, electrons may be captured by the barrier because of their energy losses via synchrotron emission in electric and magnetic fields if these fields are strong enough. In turn, such a capture of electrons may result in complete destruction of the stationary solution.

The beam – barrier collision is similar, in many respects, to collisionless shocks. Such shocks in astrophysical settings can and do accelerate charged particles to high energies (see, for a review, Refs. [19,20]). The efficiency of particle acceleration by shocks may be as high as $\sim 20 - 40$ % (e.g., Ref. [19]). This value is more or less the same as the fraction of the kinetic energy of the beam which may be transferred to high-energy electrons in the process of the beam – barrier collision.

Besides of analytical calculations (e.g., Refs. [21,22]), acceleration of particles by shocks was studied numerically in both test particle Monte Carlo simulations (see Ref. [23] and references therein) and self-consistent plasma simulations (e.g., Refs. [24–27]). Most current self-consistent simulations of plasma shocks used in astrophysics are of the hybrid type because the m_e/m_p ratio is small, $m_e/m_p \simeq 0.54 \times 10^{-3}$. In the hybrid approach, the ions are treated kinetically using standard particle-in-cell techniques, while the electrons are treated as a massless, charge neutralizing fluid. In our simulations we did not use the hybrid approach because the case of ultrarelativistic beam is, in some respects, easy than non-relativistic case. This is because in our case, $\Gamma_0 \gg 1$, electrons are accelerated fast, and the mean energy becomes only an order of magnitude smaller than the mean energy of protons. In this case, the ratio of the gyroradii of electrons and protons is about two orders of magnitude larger than m_e/m_p that is the ratio of the gyroradii of electrons and protons in non-relativistic plasma. This allowed us to treat both electrons and protons kinetically.

The configuration considered in our simulations is not quite self-consistent. Indeed, the barrier magnetic field has to be generated by some kind of current flowing in the plane $x = 0$ in the y direction. However, the evolution of this current because of its interaction with the induced electromagnetic fields was not studied. In laboratory experiments, an external current flowing along a sheet of thin wires can be the barrier-front current. As to a situation which is relevant for astrophysics, the barrier fields has to be generated by the magnetized plasma of the barrier. Numerical considerations of such a configuration are under way.

VI. ASTROPHYSICAL APPLICATIONS

There are at least two kinds of astrophysical objects to which the results of our simulations may be applied. They are the sources of γ-ray bursts and strongly collimated jets of active galactic nuclei.

A. Cosmological γ-ray bursters

Gamma-ray bursts are brief, $\sim 10^{-2} - 10^{2}$ s, bursts of high-energy radiation that appear at random in the sky, emitting the bulk of their energy in the range from ~ 0.1 MeV to a few MeV (for a review of observational data on γ-ray bursts see Ref. [28]). During their appearance, they often outshine all other sources in the γ-ray sky combined. More than two decades have passed since the discovery of γ-ray bursts, but their origin is still a mystery. The observed isotropy of γ-ray bursts in the sky and deficiency of faint bursts strongly suggest [29,30] that they are cosmological in origin [31]. A cosmological origin of γ-ray bursters implies that the typical energy output in both hard X-rays and γ-rays is about a few $\times 10^{51}$ ergs, that is, about $10^{-3} M_{\odot} c^{2}$. Such high energetics of γ-ray bursters and a short time scale of γ-ray flux variability call for very compact objects as a source of γ-ray bursts. These objects may be either fast-rotating neutron stars which arose from accretion-induced collapse of white dwarfs in binaries [4] or differentially rotating disk-like objects which are formed by the merger of a binary consisting of two neutron stars [32,33]. The strength of the magnetic field B_s at the surface of these objects may be up to $\sim 10^{16}$ G [4,6].

A common point of all acceptable models of γ-ray bursters is that a relativistic, $\Gamma_0 > 10^2 - 10^3$, wind is a source of their radiation (e.g., Refs. [34,35]). Otherwise, high-energy photons are absorbed by $\gamma + \gamma \rightarrow e^{+} + e^{-}$, and both observed durations of γ-ray bursts and their hard energy spectra, often with a very high energy tail extending up to hundreds of MeV, cannot be explained. Most probably, the radiation of γ-ray bursts is produced in the process of interaction between such a wind and an external medium [7,11]. For both the post-merger objects and fast-rotating neutron stars, the total energy of the outflowing gas cannot be more than 10^{53} ergs. Therefore, to explain the energetics of cosmological γ-ray bursters it is needed that not less than a few per cent of the wind energy is transformed into high-frequency radiation.

From our simulations of the beam – magnetic barrier collision it follows that the energy which is lost by a relativistic magnetized wind in the process of its interaction with an external medium is distributed in the following way: About half of this energy is in ultra-relativistic protons which are reflected from the wind front. The mean energy of reflected protons in the frame of the burster is $\sim m_p c^2 \Gamma_0^2$. The other half of the wind energy losses is distributed more or less evenly between low-frequency oscillations of electromagnetic fields, and both high-energy electrons and their high-frequency radiation. The low-frequency electromagnetic oscillations which are generated near the wind front can accelerate electrons to very high energies and decay at some distances from the front [36,37]. As a result of these, the fraction of the kinetic energy of relativistic magnetized winds which is transferred to high-energy electrons and then to high-frequency emission might be, in principle, as high as $\sim 40 - 50\%$. This is more than enough to explain the energetics of γ-ray bursters.

In the burster frame, the characteristic energy, $\langle \tilde{\varepsilon}_\gamma \rangle$, of photons which are generated by accelerated electrons in the vicinity of the wind front is $\sim \Gamma_0$ times higher than the value of $\langle \varepsilon_\gamma \rangle$ (see Eq. (14)) in the frame of the outflowing gas because of the Doppler effect, $\langle \tilde{\varepsilon}_\gamma \rangle \simeq \Gamma_0 \langle \varepsilon_\gamma \rangle$. Taking into account that Γ_0 has to be more than $\sim 10^2$ [2,3], from Eq. (14) we can see that the radiation which is generated near the wind front with a high enough efficiency, $\xi_\gamma \gtrsim 10^{-2}$, has the characteristic energy $\langle \tilde{\varepsilon}_\gamma \rangle \gtrsim 10^2 - 10^3$ MeV, while the main part of emission of detected bursts is in the range from a few $\times 10$ keV to a few MeV. In other words, the radiation from the front vicinity is either too hard or too weak to explain the bulk of the burst emission. The γ-ray emission which is generated near the wind front may be responsible for the high energy γ-rays, $\varepsilon_\gamma >$ a few ten MeV, which are observed in the spectra of some bursts [38].

The bulk of emission from γ-ray bursters may be explain by the synchrotron radiation of high-energy electrons which are ejected from the wind front ahead of the front. Indeed, electromagnetic fields ahead of the wind front are the fields of low-frequency electromagnetic waves which are generated near the wind front due to non-stationarity of the wind – external medium interaction. In this case, the mean value of the magnetic field is about $0.2 B_0$. The mean energy of high-energy electrons reflected from the wind front is $\sim (3-5)$ times smaller than the mean energy of radiating electrons which are responsible for the generation of γ-rays near the front. Therefore, the characteristic energy of synchrotron photons which are generated far ahead of the wind front is about hundred times smaller than the characteristic energy, $\langle \tilde{\varepsilon}_\gamma \rangle$, of photons from the front vicinity. This energy is of the order of characteristic energy of γ-ray burst emission.

B. The jets of active galactic nuclei

At radio frequencies, where VLBI can resolve the emission regions at the milliarcsecond scale, many of radio-loud active galactic nuclei (AGNs) exhibit compact jets (e.g., Ref. [1]). These jets are remarkably well collimated, with opening angles typically less than a few degrees. The Lorentz factor of the outflowing plasma is $3 \lesssim \Gamma_0 \lesssim 30$.

Recently, the Energetic Gamma Ray Experiment Telescope (EGRET) on the Compton Gamma Ray Observatory (CGRO) has detected [39] a few ten extragalactic sources, which are thought to be radio galaxies favorably oriented so that the axes of the radio jets are nearly aligned in our observing direction (e.g., Ref. [40]). The main part of the γ-ray emission from the EGRET sources is in the range from a few ten MeV to a few GeV. Besides, very hard γ-rays at TeV energies were detected from Mrk 421 with the ground-based Whipple telescope [41]. Hence, particles are accelerated in the jets of AGNs at least up to the energies of $\sim 10^9 - 10^{12}$ eV.

If the jet of AGN is free (confined solely by its own inertia), it resembles a conic section of a spherical wind. In this case, the components of the magnetic field parallel and transverse to the jet velocity are $B_\parallel \propto r^{-2}$ and $B_\perp \propto r^{-1}$, respectively, where r is the distance from the central engine which is responsible for the AGN activity. Therefore, at large distances from the engine the field of the jet is mainly across its velocity, $B_\perp \ll B_\parallel$, and our simulations may be applied to decribe the interaction between the jet front and an external medium. As it is shown above, in the process of such an interaction electrons may be accelerated to high energies, $\Gamma_e \gg \Gamma_0$. Using Eq. (12), the mean Lorentz factor of accelerated electrons in the AGN frame is $\langle\Gamma_e\rangle \sim 10^2\Gamma_0^2$. For $\Gamma_0 = 10$, that is the typical value of Γ_0 for the jets of AGNs, we have $\langle\Gamma_e\rangle \sim 10^4$.

It was suggested [42–44] that the γ-ray emission of jets is produced when high energy electrons Compton-scatter an external radiation which is either the thermal UV radiation of the accretion disk around a supermassive black hole [42] or the optical and UV emission of gas clouds surrounding the central engine [43]. In both cases the typical energy of photons which are scattered by the high energy electrons is $\varepsilon_0 \sim 1 - 10$ eV. At $\Gamma_0 = 10$, the mean energy of photons after scattering is $\sim \varepsilon_0 \langle\Gamma_e\rangle^2 \sim 0.1 - 1$ GeV, that is consistent with the data on γ-ray emission from AGNs.

For $\Gamma_0 \sim 30$, from Eq. (12) the maximum energy of accelerated electrons is $\sim m_p c^2 \Gamma_0^2 \simeq 10^{12}$ eV which is enough to explain the energies of TeV γ-rays detected [41] from Mrk 421.

ACKNOWLEDGMENTS

This research was supported by MINERVA Foundation, Munich / Germany.

---

[1] T. V. Cawthorne, in *Beams and Jets in Astrophysics*, edited by P.A. Hughes (Cambridge Univ. Press, Cambridge, 1991), p. 187.

[2] M. G. Baring, Astrophys. J. Supp. **90**, 899 (1993).

[3] R. Narayan, B. Paczyński, and T. Piran, Astrophys.J. **395**, L83 (1992).

[4] V. V. Usov, Nature (London) **357**, 472 (1992).

[5] V. V. Usov, Mon. Not. R. Astr. Soc. **267**, 1035 (1994).

[6] C. Tompson and R.C. Duncan, Astrophys. J. **408**, 194, (1993).

[7] P. Mészáros and M. J. Rees, M.J. Astrophys. J. **405**, 278 (1993).

[8] K. Papadopoulos, A. Mankofsky, R. C. Davidson, and A. T. Drobot, Phys. Fluids B **3**, 1075 (1991); A.V. Gordeev, A.S. Kingsep, and L.I. Rudakov, Physics Reports **243**, 215 (1994).

[9] Rosenbluth, M.N. In *Plasma Physics and Thermonuclear Research*, edited by C.L. Longmire, J.L. Tuck, and W.B. Thomson (Pergamon Press, 1963) Vol. 2, p. 271.

[10] W. Peter, A. Ron, and N. Rostocker, Phys. Fluids **22**, 1471 (1979).

[11] M. V. Smolsky and V. V. Usov, Astrophys. J. **461**, 858 (1996).

[12] L. D. Landau and E. M. Lifshitz, *The Classical Theory of Fields* (Pergamon Press, 1971)

[13] G.B. Rybicki and A.P. Lightman, *Radiative Processes in Astrophysics* (New York: John Wiley and Sons, 1979)

[14] M. Hoshino, J. Arons, Y. A. Gallant, and A. B. Langdon, Astrophys. J. **390**, 454 (1992).

[15] A collection of Fortran solvers for the initial value problem for ordinary differential equation systems, *http://www.netlib.org/odepack*

[16] Octave – a high-level language, primarily intended for numerical computations, *http://www.che.wisc.edu/octave/*

[17] *http://www.mathworks.com/*

[18] W. Peter, private communication.

[19] R.D. Blandford and D. Eichler, Phys. Rep. **154**, 1 (1987).

[20] F.C. Jones and D.C. Ellison, Space Sci. Rev. **58**, 259 (1991).

[21] J.R. Jokipii, Astrophys. J. **313**, 842 (1987).

[22] M. Ostrowski, Mon. Not. R. Astr. Soc. **233**, 257 (1988).

[23] M.G. Baring, D.C. Ellison, and F.C. Jones, Adv. Space Sci. **8**/9, 397 (1995).

[24] K. Guest, J. Geophys. Res. **93**, 9649 (1988).

[25] D. Burgess, Geophys. Res. Lett. **16**, 345 (1989).

[26] M. Scholer, Geophys. Res. Lett. **17**, 1821 (1990).

[27] D. Krauss-Varban and D. Burgess, J. Geophys. Res. **96**, 143 (1991).

[28] G.J. Fishman and C.A. Meegan, Ann. Rev. Astron. Astrophys. **33**, 415 (1995).

[29] M.S. Briggs, Astrophys. Sp. Sci. **231**, 3 (1995); M.S. Briggs *et al.*, Astrophys. J. **459**, 40 (1996).

[30] For another arguments in favor of cosmological origin of γ-ray bursters see B. Paczyński, Acta Astron. **41**, 257, (1991); R. Nemiroff *et al.*, Astrophys. J. **435**, L133 (1994); J.P. Norris *et al.*, Astrophys. J. **439**, 542 (1995).

[31] V. V. Usov and G. V. Chibisov, Sov. Astron. **19**, 115 (1975); S. van den Bergh, Astrophys. Sp. Sci. **97**, 385 (1983).

[32] J. Goodman, A. Dar, and S. Nussinov, Astrophys. J. **314**, L7 (1987).

[33] D. Eichler, M. Livio, T. Piran, and D. Schramm, Nature (London) **340**, 126 (1989).

[34] D.H. Hartmann, in *The Gamma-Ray Sky with Compton GRO and SIGMA*, NATO ASI Proc. No 461, edited by M. Signore, P. Salati, and G. Vedrenne (Kluwer, Dordrecht, 1995), p. 329; D.H. Hartmann, and S.E. Woosley, Adv. Space Res. **15**, (5)143, (1995).

[35] C.D. Dermer and T.J. Weiler, Astrophys. Sp. Sci. **231**, 377 (1995).

[36] J.E. Gunn and J.P. Ostriker, Astrophys. J. **165**, 523 (1971).

[37] R.M. Kulsrud, Phys. Rev. Lett. **28**, 636 (1972).

[38] K. Hurley *et al.*, Nature (London), **372**, 652 (1994).

[39] D.J. Thompson *et al.*, Astrophys. J. Suppl. **101**, 259 (1995).

[40] C.D. Dermer, in *Particle Astrophysics, Atomic Physics and Gravitation*, Proc. XXIXth Rencontres de Moriond, edited by J. Tran Thanh Van, G. Fontaine, and E. Hinds (Frontiers, Singapore, 1994), p. 47.

[41] M. Punch *et al.*, Nature (London) **358**, 477 (1992); M.S. Schubnell *et al.*, Astrophys. J. **460**, 644 (1996).

[42] C.D. Dermer and R. Schlickeiser, Astron. Astrophys. **416**, 458 (1993).

[43] M. Sikora, M.C. Begelman, and M.J. Rees, Astrophys. J. **421**, 153 (1994).

[44] The same mechanism of γ-ray emission was discussed for cosmological γ-ray bursters in A. Shemi, Mon. Not. Roy. Astron. Soc. **269**, 1112 (1994); N.J. Shaviv and A. Dar, Mon. Not. Roy. Astron. Soc. **277**, 287 (1995).

FIG. 1. Density of reversed protons in units of n_0 in run N.

FIG. 2. Energy spectrum of reversed protons at $x < -(c/\omega_{Bp})$ in run N.

FIG. 3. The beam penetration depth $x_{\rm pen}$ as a function of time t in run P (thick solid line), in run N (thin solid line), in run L (dotted line).

FIG. 4. Distribution of magnetic field in run N at the moments $t = 0$ (dotted line), $t = 7.96T_p$ (thin solid line) and $t = 15.9T_p$ (thick solid line).

FIG. 5. Angular distribution of reversed protons at $x < -(c/\omega_{Bp})$ in run N.

FIG. 6. Maximum energy of accelerated electrons (thick line) and intensity of their synchrotron radiation per unitary area of the barrier front (thin line) in run N.

FIG. 7. Energy spectrum of outflowing electrons, $v_x < 0$, in run N at the moment $t = 15.9T_p$.

FIG. 8. Schematic drawing of a plasma beam entering a magnetic barrier.

FIG. 9. Plots of the magnetic field $B_z(x)$ (thin solid line), the longitudinal electric field $E_x(x)$ (dotted line), and the x component of the four-velocity of electrons $u_{e,x}(x)$ (thick solid line) in run SR10.

FIG. 10. Plots of the proton energy (solid line) and the electron energy (dotted line) in run SR10.

FIG. 11. Numerical resolution of the main results of the stationary case, run SR10. ○ – magnetic field profile, ● – electric field profile, × – longitudal component four-velocity of electrons. Each figure stands for five integration points.

FIG. 12. The value of α as a function of α_f for both the boundary condition $E_x|_{x=x_p} = 0$ (thin line) and for the boundary condition $E_x|_{x=0} = 0$ (thick line).

TABLE I. Input parameters of simulations

Run	B_0 (G)	Γ_0 (10^3)	α	$-x_{\rm min}$ (c/ω_{Bp})	$x_{\rm max}$ (c/ω_{Bp})	$t_{\rm max}$ (T_p)
A	100	0.1	2	5	10	2.8
B	300	0.3	2	5	10	2.8
C	300	1	2	5	12	3.3
D	10^4	0.5	2	5	7	3.3
E	10^4	1	2	10	7	3.5
F	10^4	2	2	5	5	2.4
G	10^5	1	2	10	5	2.3
H	10^4	1	1	10	5	4.4
I	10^3	1	4	5	20	3.5
J	10^4	1	0.2	5	15	5.1
K	300	0.3	1/3	10	5	10.6
L	300	0.3	2/5	10	5	10.6
M	300	0.3	4/7	5	30	10.6
N	300	0.3	2/3	5	30	15.9
O	300	0.3	1	5	30	10.6
P	300	0.3	2	5	30	10.6

TABLE II. Derived parameters of simulations

Run	$\frac{\langle\Gamma_e^{\rm out}\rangle}{\Gamma_0}$	$\frac{\Gamma_{\rm e,max}^{\rm out}}{\Gamma_0}$	$\frac{\langle\Gamma_e^{\rm rad}\rangle}{\Gamma_0}$	$\frac{\langle\Gamma_p^{\rm out}\rangle}{\Gamma_0}$	ξ_γ (10^{-2})	$\langle\varepsilon_\gamma\rangle$ (MeV)
A	132	603	643	0.61	3.2×10^{-3}	0.013
B	107	785	809	0.41	0.12	0.45
C	106	464	543	0.57	0.96	5.1
D	119	745	425	0.48	3.4	8.9
E	92	542	337	0.48	11	14
F	92	785	235	0.40	12	35
G	56	402	193	0.43	14	36
H	116	801	419	0.57	9.9	15
I	105	427	555	0.41	2.9	9.1
J	9.5	39	41	0.99	0.16	0.20
K	115	573	288	0.94	0.017	0.09
L	424	1473	596	0.73	0.052	0.19
M	296	1038	913	0.69	0.18	0.64
N	489	1275	807	0.50	0.36	0.34
O	213	1284	821	0.62	0.16	0.34
P	94	550	883	0.63	0.42	0.68

TABLE III. Penetration of the beam particles with $\Gamma_0 = 300$ into the magnetic barrier with $B_0 = 300$ G for different values of α.

α	2	1	2/3	4/9	2/5	1/3
$v_{\rm pen}/c$	0.32	0.17	0.077	0.05	0	0

TABLE IV. Parameters of simulations of stationary collision between the beam with $\Gamma_0 = 300$ and the magnetic barrier for the boundary condition $E_x\|_{x=x_p} = 0$.

Run	α_f	α	$\frac{\Gamma_{p,min}}{\Gamma_0}$	$\frac{\Gamma_{e,max}}{\Gamma_0}$	$\frac{B_f}{B_0}$	$\frac{E_f}{B_0}$	$\frac{E_{max}}{B_0}$
SR1	0.01	0.0098	0.99	1.02	0.99	−0.015	−0.015
SR2	1/10	0.086	0.92	1.2	0.92	−0.13	−0.13
SR3	1/5	0.15	0.86	1.3	0.87	−0.22	−0.22
SR4	1/2	0.29	0.76	2.1	0.76	−0.40	−0.41
SR5	1	0.44	0.67	7.1	0.67	−0.57	−0.58
SR6	2	0.50	0.64	48	0.50	−0.50	−0.62
SR7	4	0.51	0.64	97	0.36	−0.38	−0.61
SR8	10	0.51	0.63	170	0.23	−0.27	−0.58
SR9	40	0.51	0.63	276	0.11	−0.20	−0.53
SR10	1000	0.51	0.62	434	0.023	−0.14	−0.45

TABLE V. Parameters of simulations of stationary collision between the beam with $\Gamma_0 = 300$ and the magnetic barrier for the boundary condition $E_x\|_{x=0} = 0$.

Run	α_f	α	$\frac{\Gamma_{p,max}}{\Gamma_0}$	$\frac{B_f}{B_0}$	$\frac{E_x(x_p)}{B_0}$
SL1	0.01	9.8×10^{-3}	1	0.99	0.016
SL2	1/10	0.082	1.06	0.90	0.15
SL3	1/5	0.13	1.1	0.81	0.29
SL4	1/3	0.16	1.3	0.69	0.45
SL5	1/2	0.15	1.5	0.55	0.63
SL6	2/3	0.11	1.9	0.41	0.78
SL7	3/4	0.085	2.2	0.34	0.85
SL8	0.8	0.068	2.5	0.29	0.88
SL9	0.9	0.032	3.7	0.19	0.95
SL10	1	4.6×10^{-4}	31	0.02	1

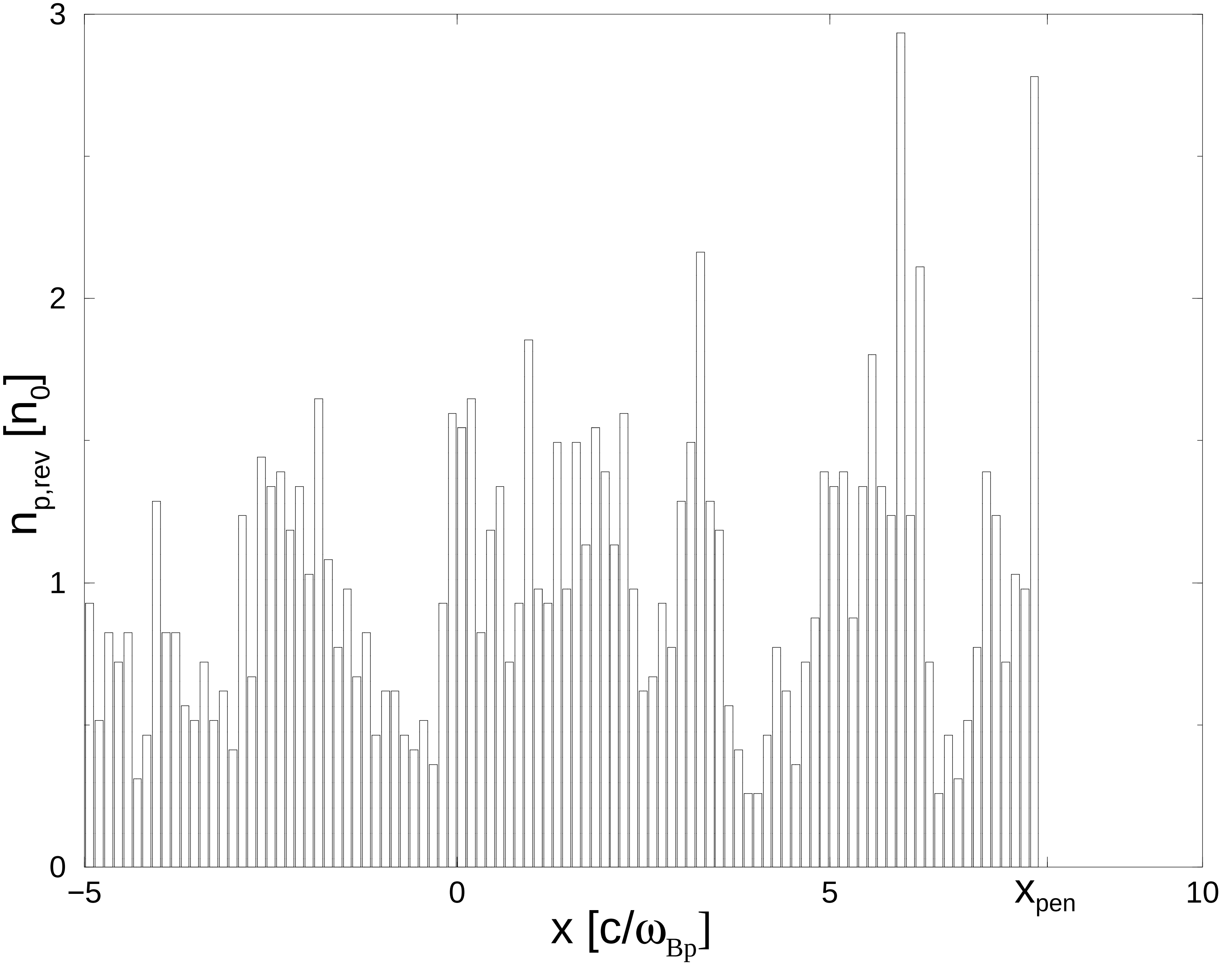
$n_{p,rev}$ [n_0]
3
2
1
0
−5
0
5
x_{pen}
10
x [c/ω_{Bp}]

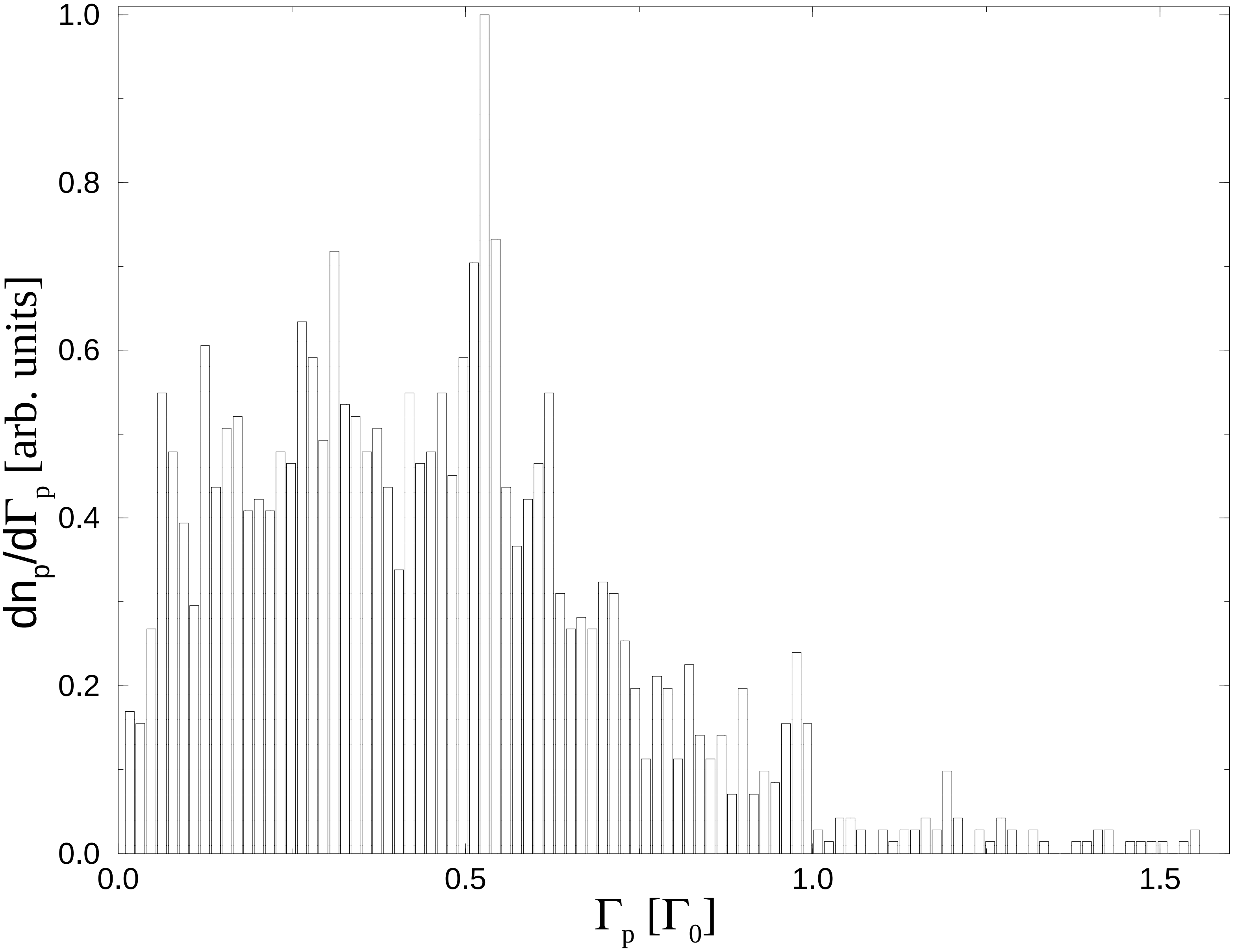
1.0
0.8
0.6
0.4
0.2
0.0
0.0
0.5
1.0
1.5
$dn_p/d\Gamma_p$ [arb. units]
Γ_p [Γ_0]

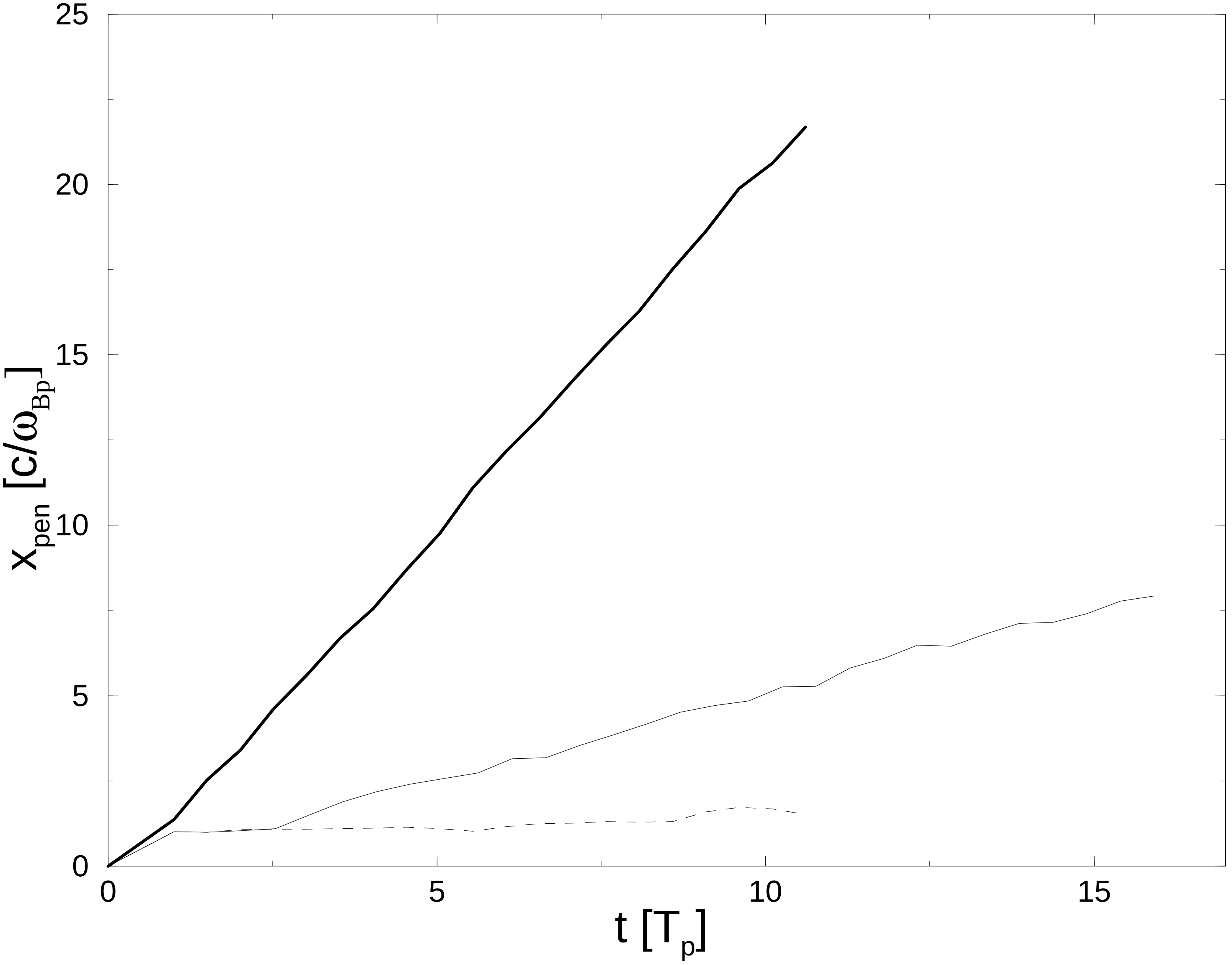

25
20
15
10
5
0
0
5
10
15
x_{pen} [c/ω_{Bp}]
t [T_p]

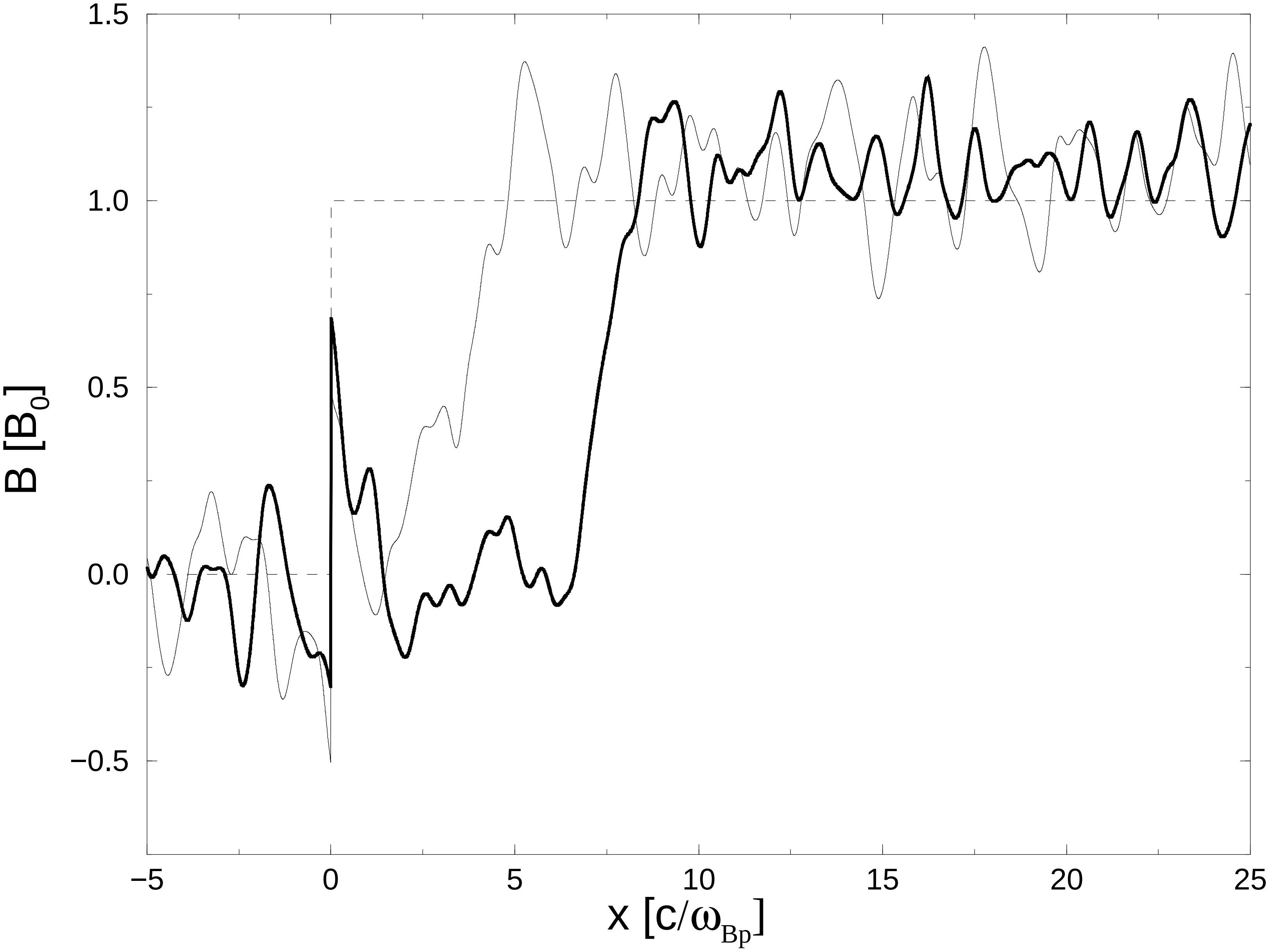
1.5
1.0
0.5
0.0
−0.5
B [B_0]
−5
0
5
10
15
20
25
x [c/ω_{Bp}]

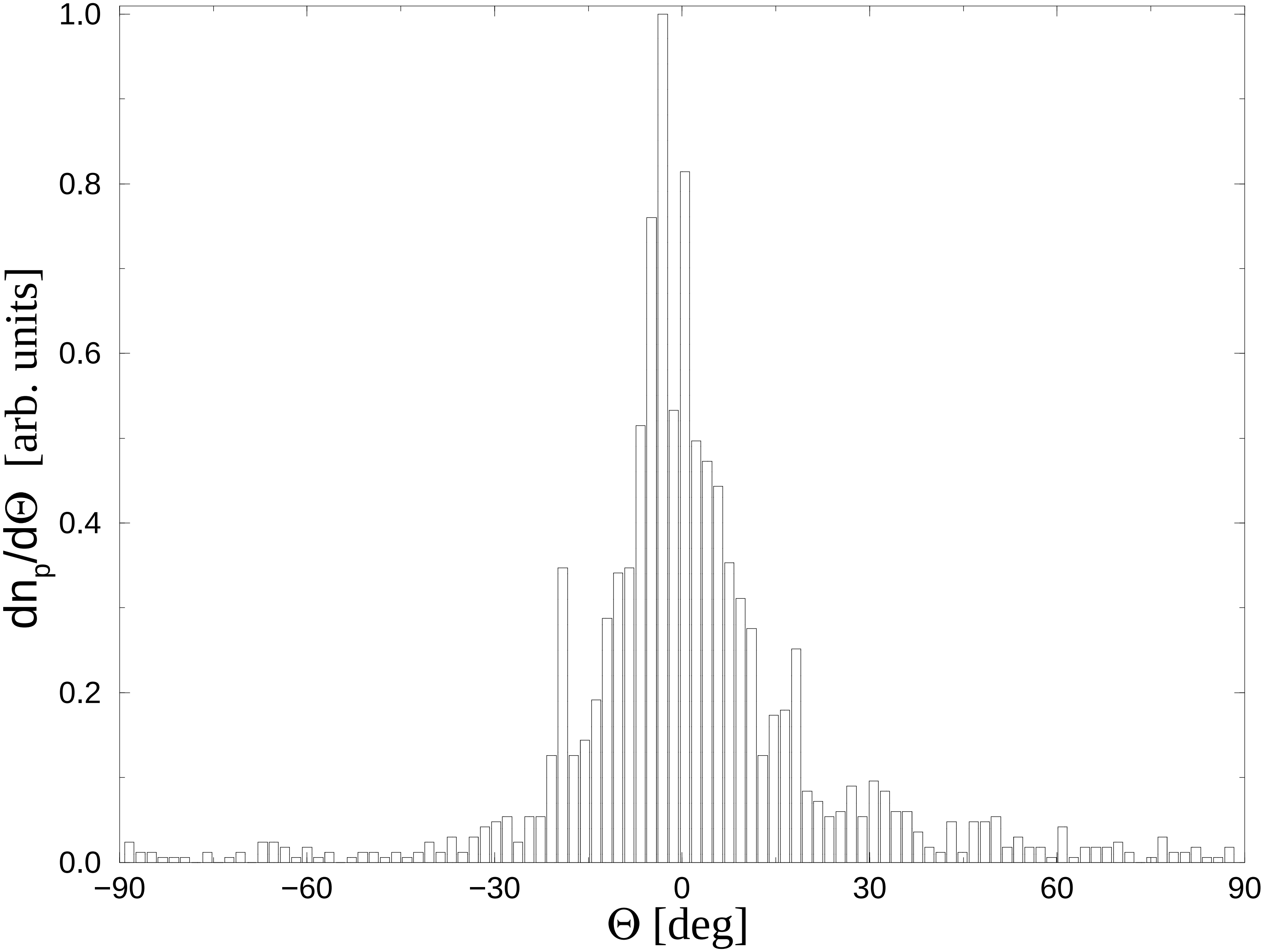

dn$_p$/dΘ [arb. units]
1.0
0.8
0.6
0.4
0.2
0.0
−90
−60
−30
0
30
60
90
Θ [deg]

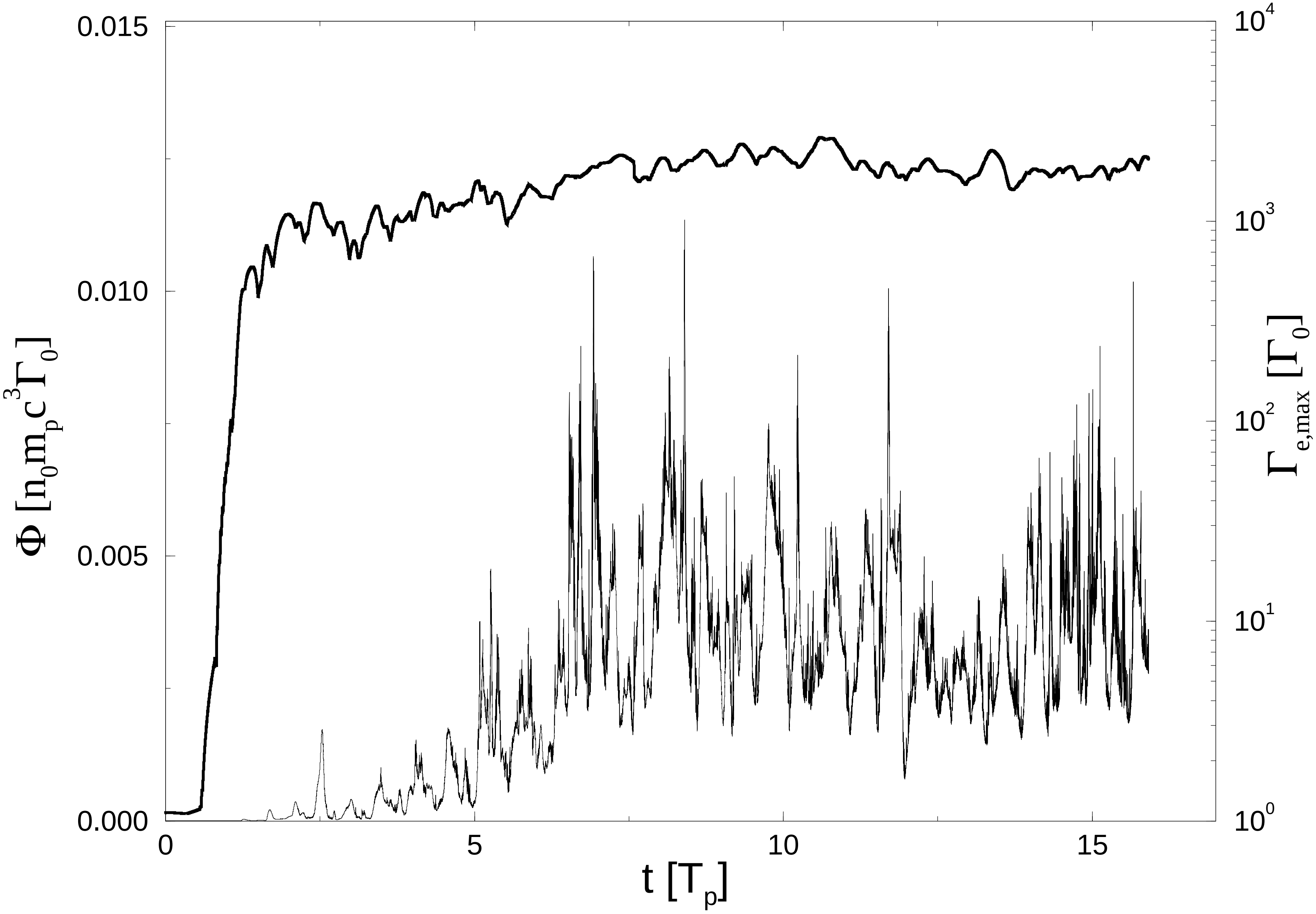
0.015
0.010
0.005
0.000
$\Phi\ [n_0 m_p c^3 \Gamma_0]$
0
5
10
15
$t\ [T_p]$
10^4
10^3
10^2
10^1
10^0
$\Gamma_{e,max}\ [\Gamma_0]$

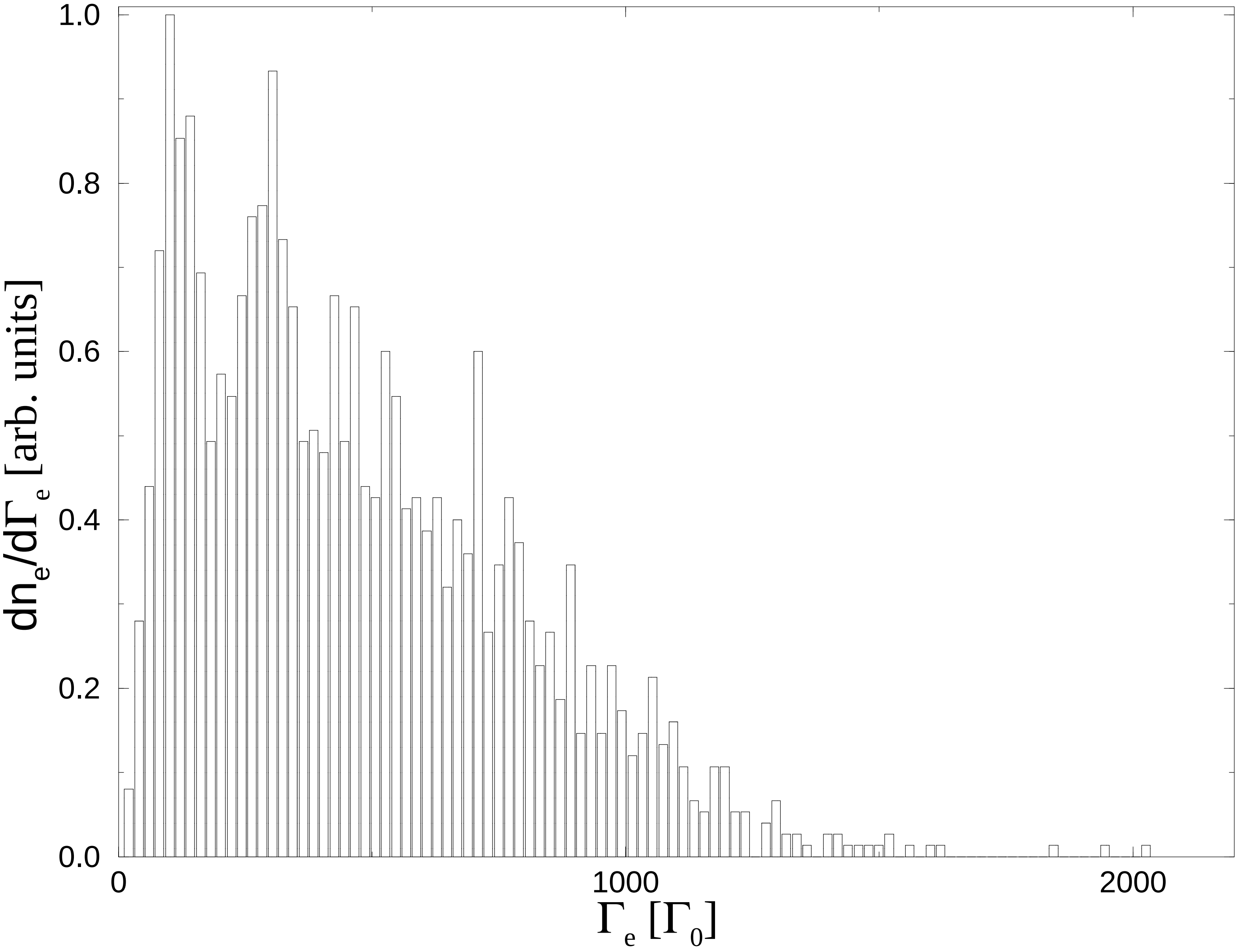

1.0
0.8
0.6
0.4
0.2
0.0
0
1000
2000
$dn_e/d\Gamma_e$ [arb. units]
Γ_e [Γ_0]

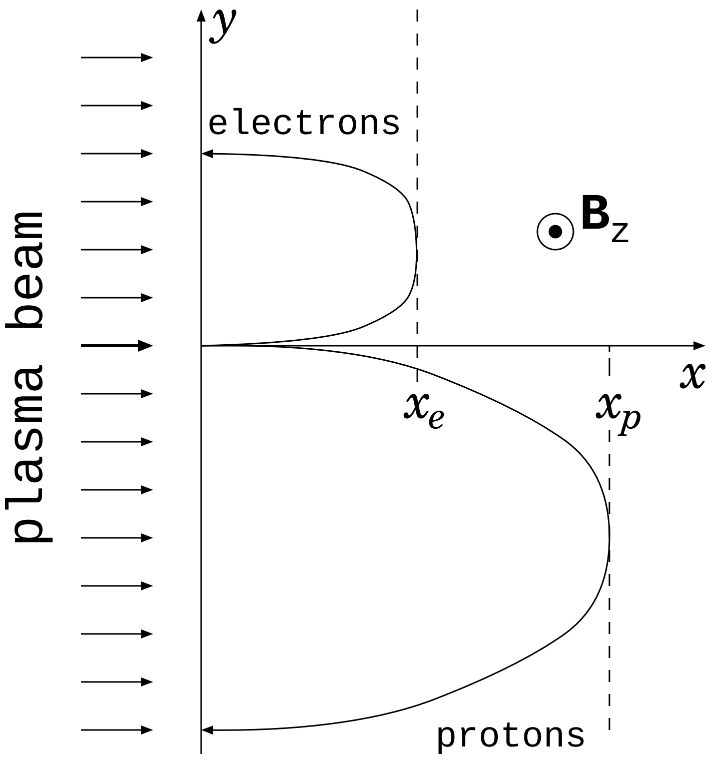
y
electrons
B_z
plasma beam
x
x_e
x_p
protons

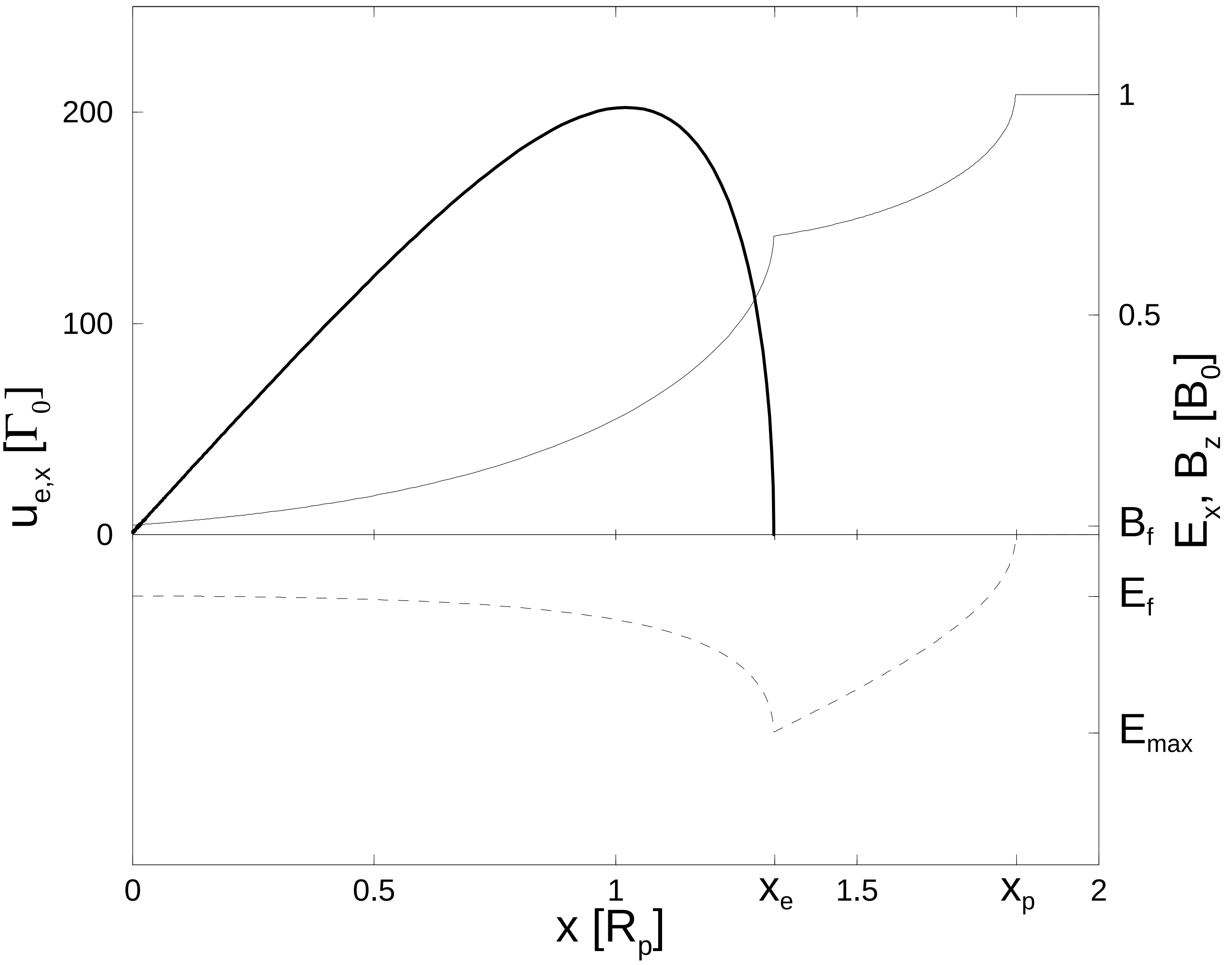
200
100
0
$u_{e,x}$ [Γ_0]
1
0.5
B_f
E_f
E_{max}
E_x, B_z [B_0]
0
0.5
1
x_e
1.5
x_p
2
x [R_p]

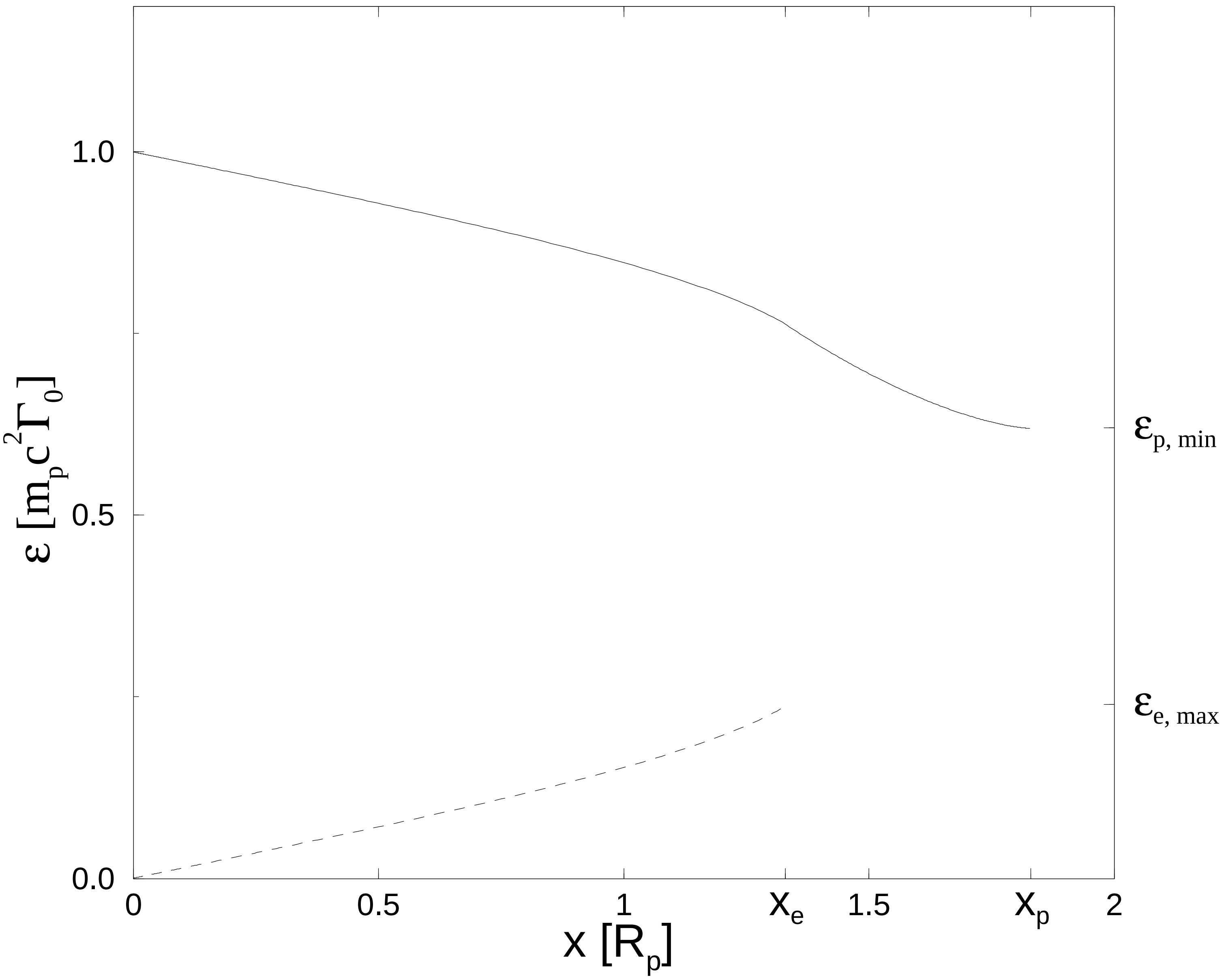
1.0
0.5
0.0
$\varepsilon\ [m_p c^2 \Gamma_0]$
0
0.5
1
x_e
1.5
x_p
2
$x\ [R_p]$
$\varepsilon_{p,\ min}$
$\varepsilon_{e,\ max}$

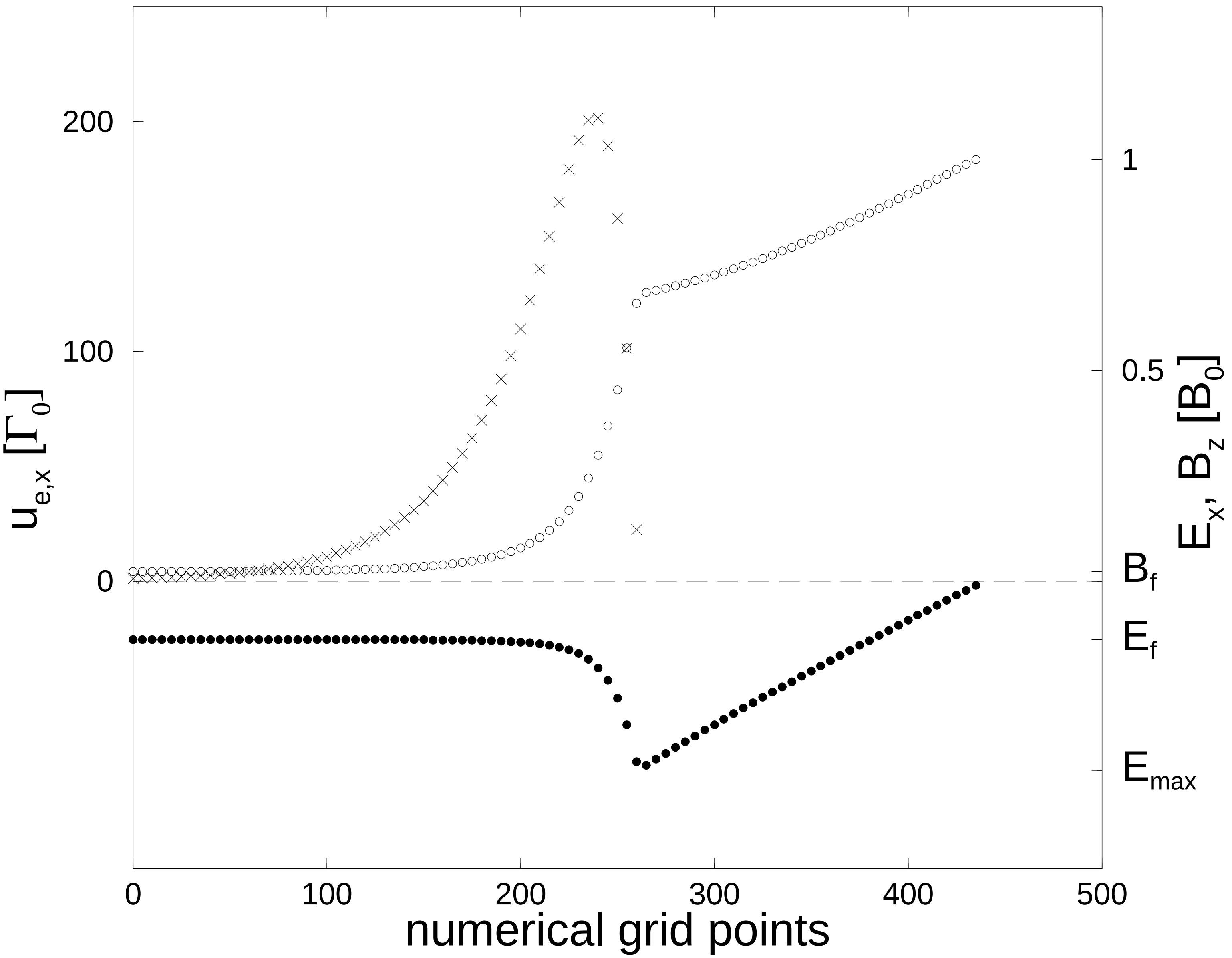
200
100
0
$u_{e,x}$ [Γ_0]
1
0.5
B_f
E_f
E_{max}
E_x, B_z [B_0]
0
100
200
300
400
500
numerical grid points

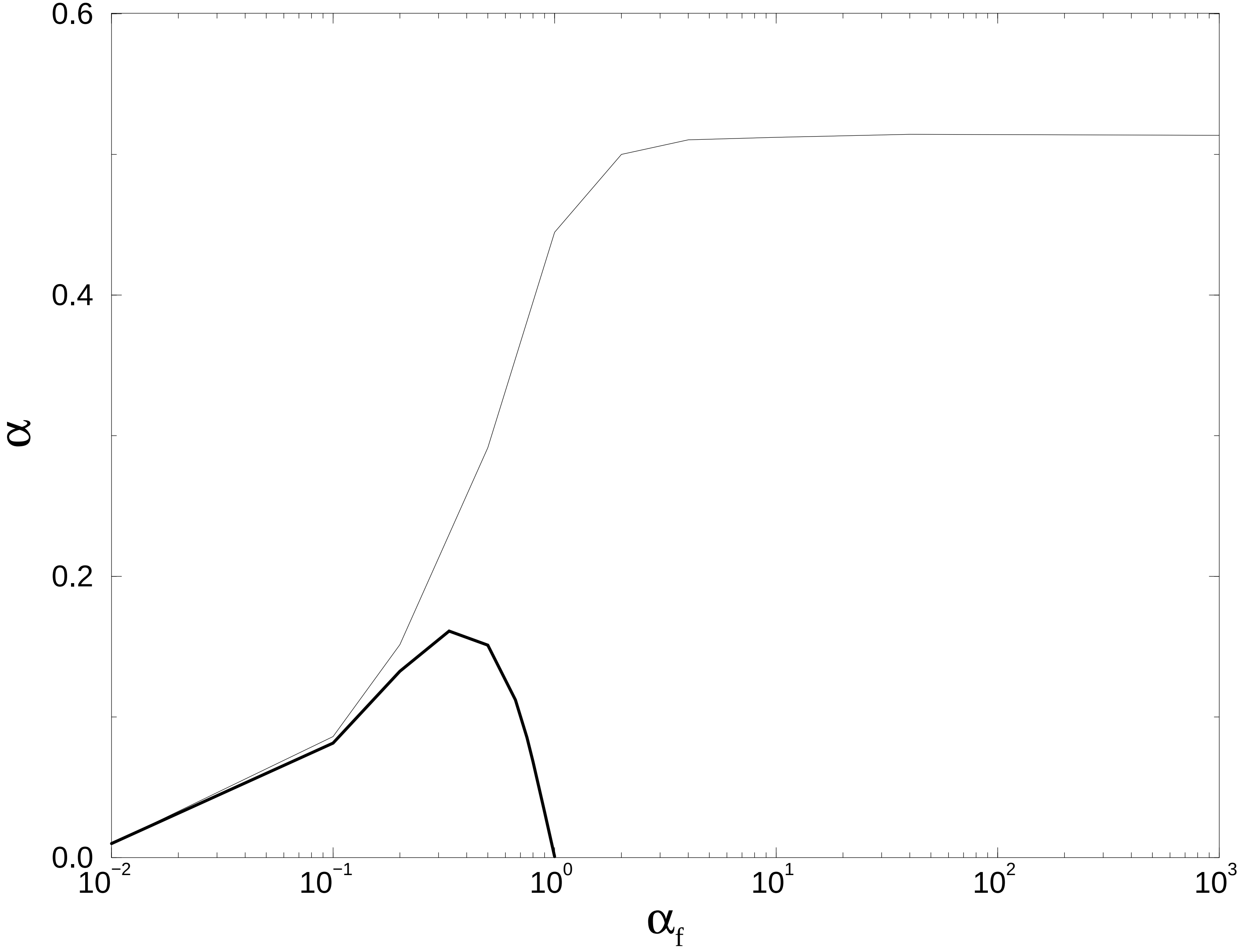
0.6
0.4
0.2
0.0
α
10^{-2}
10^{-1}
10^{0}
10^{1}
10^{2}
10^{3}
α_f